

polysilicon for solar cell use. The process involves deposition of a sandwich structure in which an intermediate sacrificial layer of carbon is oxidized out. The kinetics of this process were shown to be diffusion controlled, and the effects of several primary and secondary variables as well as optimal process conditions are given. Although close agreement between theoretical and experimental under-cut rates was not obtained, the theory provides a framework for interpreting the results and predicting the effects of process changes.

Acknowledgments

Thanks are due to Motorola, Incorporated, for permission to publish this work, and to the Gasonics Company for performing the high pressure oxidations. This work was performed at Solavolt International, which was a partnership of Motorola Solar Energy, Incorporated and SES, Incorporated, a subsidiary of Shell Oil Company. A patent is pending on this process.

The Kinetics of Tungsten Etching by Atomic and Molecular Chlorine

M. Balooch, D. S. Fischl, and D. R. Olander

University of California, Berkeley, California 94720

W. J. Siekhaus

Lawrence Livermore National Laboratory, Livermore, California 94550

ABSTRACT

The reactions of atomic and molecular chlorine with tungsten were studied by modulated beam-mass spectrometric methods over the temperature range 300-1350 K. The atomic beam was generated by an RF plasma discharge. With both atomic and molecular beams, the main reaction product up to about 1000 K was WCl_4 . The reaction probability with atomic chlorine was a factor of approximately ten higher than that obtained with molecular chlorine. The reaction was nonlinear with respect to Cl_2 intensity at low beam fluxes but approached linearity at high beam intensities. Above 1000 K the main reaction product was atomic chlorine. Its reaction probability increased rapidly with temperature; at 1300 K nearly complete dissociation of Cl_2 was observed. A kinetic model based on the Eley-Rideal mechanism was proposed and compared with the data.

Refractory metals are integral components of advanced electronic devices. Their low resistance, high temperature stability, and amenability to dry etch patterning make them useful as interconnects and gates for VLSI applications.

In the accompanying paper (1), etching of tungsten films by atomic chlorine downstream of a plasma discharge is reported.

In the present work, the reaction of atomic and molecular chlorine with bulk tungsten was studied by modulated beam mass spectrometry. A review of the desirable features and limitations of the method are presented elsewhere (2-5). This technique is well suited for mechanistic studies because the beam modulation feature provides a direct measure of characteristic response times of the surface processes and because mass spectrometric detection permits identification of the chemical composition of the volatile reaction products.

Experimental

The apparatus, which is a slightly modified version of the one described previously (5), is shown in Fig. 1. It consists of three differentially pumped vacuum chambers separated by beam-forming orifices. The incident reactant beam is generated by effusion from a quartz source tube which has a 1 mm hole in its end. An RF discharge, in the 1.3 cm diam quartz tube 5 cm from the end containing the hole, produces the atomic chlorine reactant. The discharge is powered by a Tegal Corporation 300W RF power supply. The electrodes consist of 6 mm wide copper bands placed

Manuscript submitted Sept. 14, 1987; revised manuscript received Dec. 29, 1987.

REFERENCES

1. K. E. Petersen, *IEEE Trans. on Electron Devices*, **ED-25**(10), 1241 (1974).
2. R. T. Howe and R. S. Muller, *ibid.*, **ED-33**(4), 499 (1986).
3. R. W. Gurtler, A. Baghdadi, R. J. Ellis, and I. A. Lesk, *J. Electron. Mater.*, **7**, 441 (1978).
4. R. B. Bird, W. E. Stewart, and E. N. Lightfoot, "Transport Phenomena," p. 504, John Wiley & Sons, Inc., New York (1960).
5. R. B. Bird, W. E. Stewart, and E. N. Lightfoot, "Transport Phenomena," pp. 503-505, John Wiley & Sons, Inc., New York (1960).
6. R. C. Reid, J. M. Prausnitz, and T. K. Sherwood, "The Properties of Gases and Liquids," 3rd ed., p. 565, McGraw Hill, Inc., New York (1977).
7. T. Suzuki, A. Mimura, and T. Ogawa, *This Journal*, **124**, 1776 (1977).

outside to the tube. The spacing between the bands is 6 mm, and the discharge area is surrounded by a metal box for RF shielding. A rotating-toothed disk imparts a periodicity of 20-700 Hz to the mixed atomic and molecular beam effusing from the quartz tube. The modulation frequency is detected by an optical switch for transmission to the phase-sensitive detection electronics.

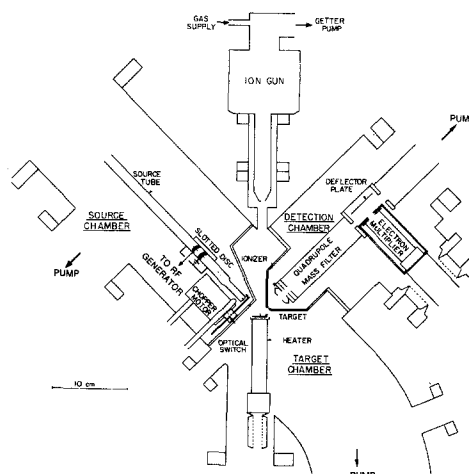


Fig. 1. Modulated beam apparatus for investigation of the reactions of tungsten with chlorine atoms and molecules.

A 1 mm diam collimator shapes this modulated flow into a thin pulsed beam of molecules or atoms. The beam is approximately 3 mm in diameter as it strikes the target surface which is held in the target chamber.

The target is polycrystalline tungsten heated by electron bombardment and the surface temperature is measured by an infrared pyrometer. The target chamber is pumped by a turbo molecular pump (1500 l/s) to a typical base pressure of 1×10^{-9} torr. Prior to an experiment, the tungsten specimen is heated to ~ 1500 K for one-half hour to remove surface oxides. After the surface is cooled to room temperature, it is ion-bombarded to remove carbon impurities.

During an experiment, part of the reactant beam merely scatters from the surface without interaction with the sample. The rest chemisorbs on the surface and eventually reappears as products. Small fractions of the reflected reactant beam and the desorbed reaction products pass in free-molecular flow through an orifice leading to the third chamber, which houses a quadrupole mass spectrometer with a line of sight view of the reaction spot on the tungsten surface.

The output from the mass spectrometer is processed by a lock-in amplifier with a two-phase accessory to yield the first Fourier components of the signal at a selected mass number. The apparent reaction probability ϵ , is the ratio of the product and reactant signals, which are corrected for the ionization efficiencies of the mass spectrometer. The phase lag ϕ is the difference between the phase angles of the product and the reactant. These are obtained from the information provided by the lock-in amplifier (2). A complete set of molecular beam data consists of measurements of ϵ and ϕ as functions of the three controllable experimental variables: the surface temperature (T), the modulation frequency of the beam (f), and the beam intensity at the sample surface (I_1 for atomic chlorine Cl and I_2 for molecular chlorine Cl_2). In conducting experiments, one variable is changed while the other two are kept constant.

Atomic Beam Generation

With the RF discharge on, the intensity of the atomic chlorine beam striking the surface is estimated by mass spectrometer detection of the reflected Cl^+ and Cl_2^+ signals from a quartz target on which Cl recombination is negligible. Both signals are insensitive to variations of the quartz target temperature, suggesting low thermal accommodation coefficients for both species on this surface. Thus the quartz surface acts simply as a reflector without changing the properties of the incident beam.

As shown in the Appendix, the intensities of the Cl_2 and Cl components of the flux impinging on the target can be determined by measuring the signals of Cl^+ and Cl_2^+ with

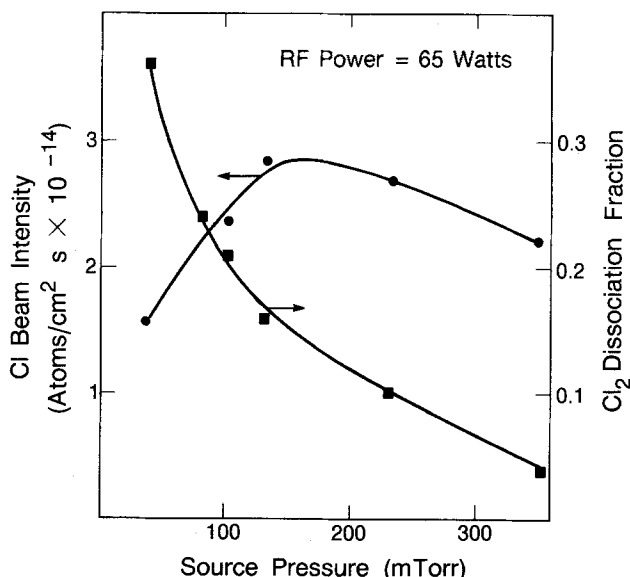


Fig. 2. Chlorine atom beam intensity and Cl_2 dissociation fraction as functions of source pressure at constant RF power of 65W.

the discharge on and with it off. The ratio of the total ionization cross sections of Cl and Cl_2 is also required. Figure 2 shows the atomic chlorine beam intensity and the dissociation fraction as functions of the gas pressure in the source tube, for a constant RF power of 65W. The total Cl plus Cl_2 effusion from the source increases with pressure; but, the dissociation fraction decreases rapidly, resulting in a maximum atomic beam intensity of $\sim 3 \times 10^{14}$ atom/ $\text{cm}^2\text{-s}$ at approximately 150 mtorr pressure. When the low pressure restriction required to operate the discharge is absent, pure Cl_2 beams with intensities two orders of magnitude higher are obtained.

Results

With the tungsten sample in place, the ions containing tungsten observed by the mass spectrometer are WCl_4^+ , WCl_2^+ , WCl^+ , and W^+ . For both the atomic and molecular beams, these ions all have the same phase angle and the same dependence on surface temperature. This behavior indicates that all ions are part of the cracking patterns of WCl_4 , which is therefore the sole volatile product of the reactions up to 1000 K. Since it has the highest intensity, all measurements are performed on the WCl_2^+ peak. It is then corrected for the fragmentation pattern to yield the WCl_4 emission rate from the tungsten surface.

Discharge on, low source pressure.—The apparent reaction probabilities and phase lags of WCl_4 for atomic and molecular beams are shown as functions of temperature for a fixed chopping frequency and beam intensity in Fig. 3 and 4. The results show that the reactivity of atomic chlorine is more than an order of magnitude higher than that of molecular chlorine. The apparent reaction probabilities appear to be temperature-independent up to approximately 600 K and decrease with temperature above this point. Within experimental error, the product phase lags are the same for both the molecular and atomic beams, although they increase with increasing temperature. The curves in Fig. 3-9 are model fits and are discussed in the section on Discharge off, high source pressure.

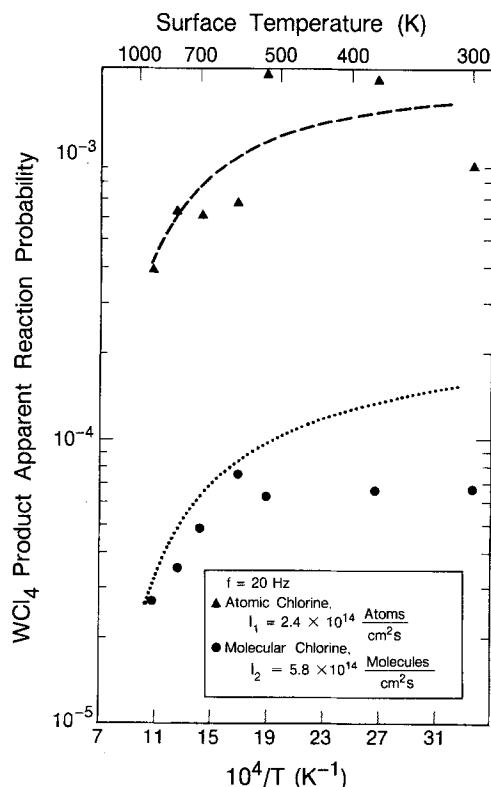


Fig. 3. WCl_4 product reaction probability for atomic (triangles) and molecular (circles) chlorine as a function of surface temperature for fixed chopping frequency of 20 Hz and beam intensities of $I_1 = 2.4 \times 10^{14}$ atom/ $\text{cm}^2\text{-s}$ and $I_2 = 5.8 \times 10^{14}$ molecules/ $\text{cm}^2\text{-s}$. The dashed curve depicts the behavior predicted by the model for atomic chlorine and dotted curve for molecular chlorine.

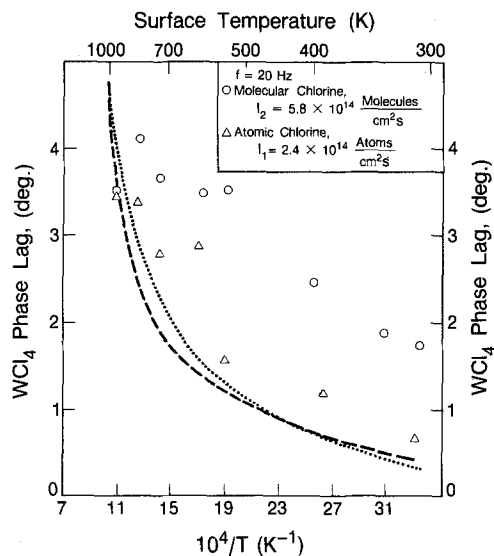


Fig. 4. WCl_4 phase lag for atomic (triangles) and molecular (circles) chlorine as a function of surface temperature for fixed chopping frequency of 20 Hz and beam intensities of $I_1 = 2.4 \times 10^{14}$ atom/cm²-s and $I_2 = 5.8 \times 10^{14}$ molecules/cm²-s. The dashed curve depicts the behavior predicted by the model for atomic chlorine and dotted curve for molecular chlorine.

Discharge off, high source pressure.—The WCl_4 reaction probabilities and phase lags as functions of the three controllable variables (surface temperature, beam intensity, and chopping frequency) are shown in Fig. 5, 6, and 7. From the phase lag results (Fig. 5), the reaction time appears to increase with increasing temperature. At a constant temperature and chopping frequency, Fig. 6 shows that the reaction is nonlinear with Cl_2 beam intensity at low values, but approaches linearity above $\sim 2 \times 10^{16}$ molecules/cm²-s. Finally, the phase lag is shown in Fig. 7 to decrease with increasing chopping frequency.

At temperatures higher than 1000 K, the main species in the reflected reaction product beam is atomic chlorine. Its reaction probability increases and its phase lag decreases sharply with increasing surface temperature. At 1353 K total dissociation of the incident molecular beam is observed (Fig. 8). Figure 9 shows that the reaction probability remains close to unity up to a beam intensity of 4×10^{16} molecules/cm²-s. Higher beam intensities result in a reduction of the reaction probability. A small phase lag increase is observed with increasing beam intensity.

Reaction Model

W-Cl₂.—The following reaction model is based primarily on data from the molecular Cl_2 beam experiments. Its form is dictated by the following features of the experimental results: (i) the existence of two reaction channels—one to

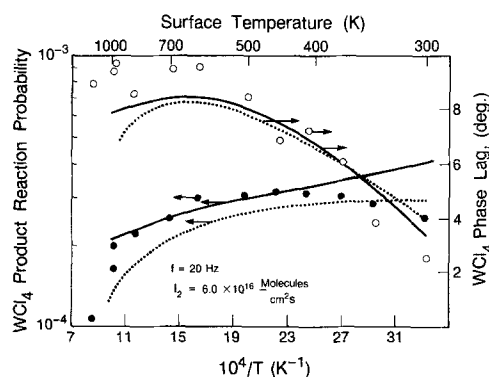


Fig. 5. Variation of WCl_4 product reaction probability and phase lag with surface temperature at a constant beam intensity of 6.0×10^{16} molecules/cm²-s and chopping frequency of 20 Hz. As described in the text, the solid and dotted curves are the model predictions for different parameters.

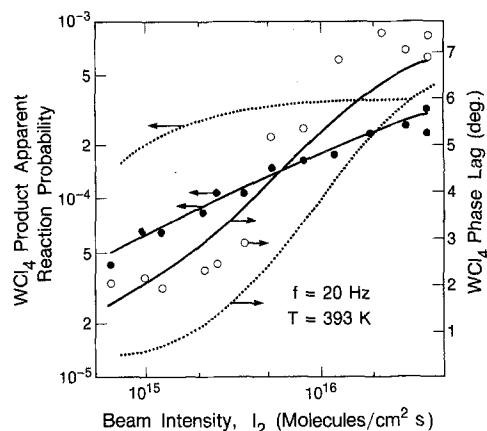


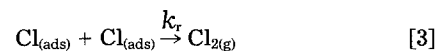
Fig. 6. Beam intensity variation of the WCl_4 product reaction probability and phase lag at a surface temperature of 393 K and a chopping frequency of 20 Hz. As described in the text, the solid and dotted curves are the model predictions for different parameters.

provide WCl_4 at low temperatures and the other leading to Cl at high temperatures; (ii) the nonlinearity of the reaction producing WCl_4 at low beam intensities and the approach to linearity at higher beam intensities; (iii) the lower phase lag of WCl_4 compared to that of Cl up to 1300 K (Fig. 5, 8); and (iv) the decrease of the WCl_4 phase lag with increasing chopping frequency.

Reaction starts with dissociative chemisorption of molecular chlorine. This reaction is characterized by a sticking probability of η on the bare portion of the tungsten surface and is given by the following



where θ is the coverage of chemisorbed chlorine atoms. The remaining elementary reaction steps in the model are the following



where reaction [2] represents the desorption of chemisorbed chlorine atoms with a rate constant k_d . Recombination of the surface Cl leading to desorption as molecular chlorine is described by reaction [3] (with rate constant k_r). Note that the Cl_2 product of this reaction step cannot be detected because it is mixed with Cl_2 from the incident beam which has reflected from the surface. The rate con-

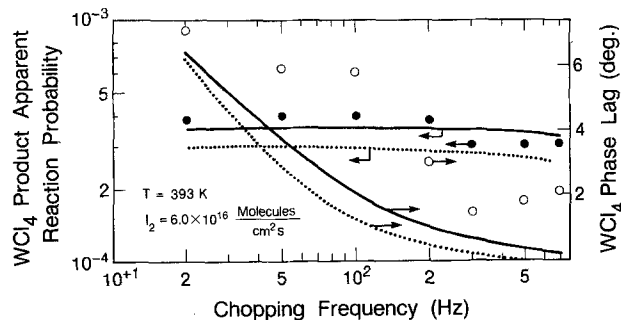


Fig. 7. Modulation frequency dependence of the WCl_4 product reaction probability and phase lag at a surface temperature of 393 K and a beam intensity of 6.0×10^{16} molecules/cm²-s. As described in the text, the solid and dotted curves are the model predictions for different parameters.

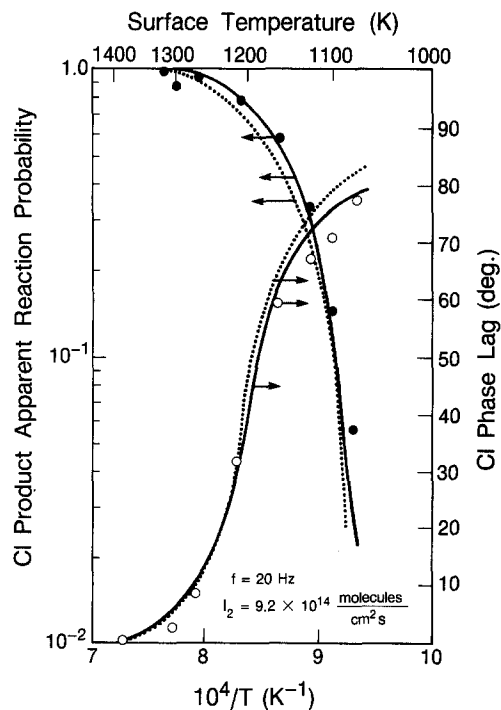


Fig. 8. Apparent reaction probability and phase lag of the atomic chlorine product as functions of surface temperature above 1000 K. The molecular beam intensity and chopping frequency are indicated. As described in the text, the solid and dotted curves are the model predictions for different parameters.

stant for reaction [3] is dependent on surface coverage and is given by

$$k_r = k_r^0 \exp \frac{[-E_r(1 - g^0\theta)]}{RT}$$

where k_r^0 , E_r , and g^0 are constants. Finally, the production of WCl_4 is assumed to be by an Eley-Rideal mechanism. In reaction [4], a chlorine molecule from the gas-phase strikes a tungsten surface atom that is attached to two chemisorbed chlorine atoms. The product from this reaction is WCl_4 , which immediately desorbs. This step is characterized by a reactive sticking probability η_{er} .

At high temperatures the Cl coverage is negligible, so the active channel is the desorption of atomic chlorine represented by reaction [2], which is linear in Cl (ads). As the temperature is reduced the atomic chlorine coverage increases, shifting the reaction towards the second-order processes of Cl_2 and WCl_4 production.

A mass balance on the chemisorbed chlorine results in

$$\frac{d\theta}{dt} = \frac{2\eta I_2}{N} g(t)(1 - \theta) - 2k_r N \theta^2 - k_d \theta - \frac{2\eta_{er} I_2}{N} g(t)\theta \quad [5]$$

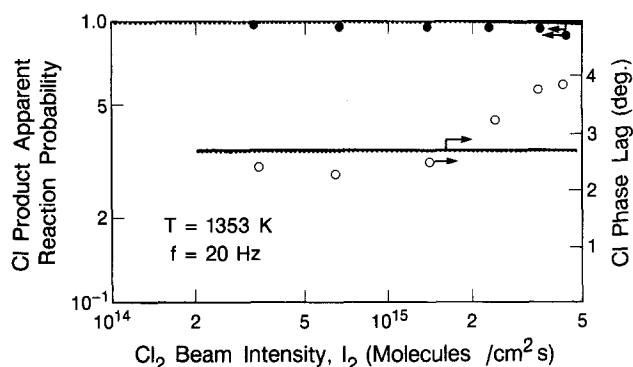


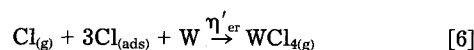
Fig. 9. Beam intensity dependence of the Cl product apparent reaction probability and phase lag at 1353 K and a chopping frequency of 20 Hz. As described in the text, the solid and dotted curves are the model predictions for different parameters. The two curves are nearly coincident.

where $g(t)$ and N are the gating function of the chopper and the maximum available sites for chlorine adsorption on the tungsten surface (1.5×10^{15} atom/cm²), respectively. I_2 is the intensity of the incident Cl_2 beam.

The first term on the right-hand side of Eq. [5] represents the supply of chlorine atoms to the surface by dissociative adsorption. Sticking is assumed to occur only on exposed surfaces. The second and third terms are the losses due to recombination and to atomic desorption. The last term is the loss through the production of WCl_4 .

Solution of Eq. [5] is accomplished by the Fourier expansion method outlined in Ref. (5, 6). The model predictions are obtained in the form of reaction product vectors, which are ratios of the product emission rates ($\eta_{er} I_2 \theta g(t)$ for WCl_4 and $k_d N \theta$ for Cl) to the incident beam impingement rate [$I_2 g(t)$]. The scalar components of the reaction product vectors are the apparent reaction probabilities and phase lags.

W-Cl.—For the beam containing atomic chlorine reactant the same reaction steps presented for the molecular beam are assumed except reaction [4] is replaced by the following



This step represents production and desorption of WCl_4 by an Eley-Rideal mechanism, with a reactive sticking probability η'_{er} . In addition, Eq. [1] is replaced by chemisorption of $\text{Cl}_{(g)}$ with unit sticking probability but preserving the same coverage dependence.

Discussion

Fitting the data to the reaction model.—The model of the tungsten reaction with molecular chlorine described in the previous section contains nine parameters. Based on past experience, the sticking probability of reaction [1] and the reaction probability characterizing the Eley-Rideal step of reaction [4] are assumed to be independent of temperature. Since almost total dissociation of Cl_2 was observed (by monitoring the reflected Cl_2 signal) above 1300 K, the bare surface sticking probability is assumed to be unity. In the absence of an energy barrier to Cl_2 adsorption on the surface, the binding energy of atomic chlorine to the tungsten surface (activation energy of k_d) should be equal to one-half the activation energy for the recombinative desorption given by in reaction [3] (E_r) plus one-half the Cl—Cl bond strength (57 kcal/mol). What remains is a five-parameter theoretical model to be fitted to the ensemble of the data displayed in Fig. 3-9. Specification of the five parameters in the model (η_{er} , k_r^0 , E_r , g^0 , and the pre-exponential factor of k_d) leads to theoretical values of ϵ and ϕ as functions of the independent variables T , f , I_2 . The predictions are compared to the data by means of error measures for the reaction probability and the phase lag. The former is defined as the sum over all data points of the square of the deviation of the data point from the model prediction for the particular set of parameters chosen. For the latter error measurement, the sum of the absolute differences between the predicted and measured phase lags is used. The method of combining the ϵ -error and the ϕ -error to produce a single measure of the global error or "goodness of fit" is arbitrary. Our method is to consider a 10% error in ϵ to be equivalent to a ten degree error in ϕ .

With this fitting algorithm, a single goodness-of-fit measure is obtained for each set of five parameters used in the theoretical model. By randomly varying the parameters, a surface representing the goodness-of-fit measure of the five-dimensional space of the model parameters is generated. A well-defined minimum is a unique deep depression in this surface.

As in most situations in which a model with many parameters is fitted to a limited quantity of data, a clear-cut minimum is seldom found. Frequently, the error surface exhibits a trough along which combinations of two (or more) parameters give equally good fits to the data. In this event, physical judgement is needed to select the "best" combination of parameters. This is precisely what occurs in the present situation. Nearly equivalent fits to the data can be obtained over a wide range of combinations of the

parameters characterizing the recombinative desorption rate constant k_r . The solid curves in Fig. 5-9 represent data fits using $k_r^0 = 10^{-13}$ cm²/s, $E_r = 2.3$ kcal/mol and $g^0 = 0$. The dotted curves in Fig. 5-9 show the fits obtained with the parameters having the values listed in Table I. The latter fit is not as good as the fit using the first set of parameters, but the first set of parameters includes a pre-exponential factor (k_r^0) which is far too small to be physically acceptable. Consequently, the parameters listed in Table I constitute the recommended set.

Using the parameters determined for the Cl₂ reaction, the best fit to the temperature dependence of ϵ and ϕ for the atomic chlorine reactions is obtained with η'_{er} of reaction [6] equal to 3×10^{-3} . This value is ~ 10 times greater than the corresponding Eley-Rideal reaction probability determined for Cl₂, which is expected due to the reactive nature of the dissociated chlorine gas. The model results are shown as the dashed curves in Fig. 3 and 4.

Desorption rate constants.—The principal results obtained by modeling the molecular beam data are the rate constants for atomic and molecular desorption (reactions [2] and [3], respectively) and are listed in Table I.

The pre-exponential factor for the atomic chlorine desorption rate constant (k_d in Table I) is in the range expected for the vibration frequency of single atoms bound to the surface. The Cl-W binding energy of 59 kcal/mol and its pre-exponential factor of 6×10^{12} s⁻¹ are compared in Table II with values deduced from the literature (7-12) for tungsten. Reference (7) reports an activation energy of nearly 94 kcal/mol for all orientations studied. On the other hand, the thermal desorption studies of Bonczek *et al.* (8) suggest a strong orientation dependence ranging from 32 kcal/mol for the densely packed (110) surface to 92 kcal/mol for the (111) surface. The calculated results (9) also suggest a lower value for the (100) surface.

Also listed in Table I is the value of the rate constant for surface chlorine recombination, k_r . The pre-exponential factor of k_r (0.02 cm²/s) is at the upper range of analogous factors for other biomolecular surface recombination steps (13-15) and is close to the rate constant for the collision frequency of a two-dimensional ideal gas (13).

Repulsive forces between nearest-neighbor surface chlorine atoms gives rise to the coverage dependence of the heat of recombinative desorption. This tends to lower the effective potential barrier for the release of the molecule to the gas phase (15, 16). A similar coverage-dependence was found for the bismuth-chlorine reaction (17, 18).

For atomic desorption, coverage-dependence is not observable, since Cl is detectable only at high temperatures where the surface is sparsely covered with chlorine.

Using a modulated molecular beam technique and monitoring only the scattered Cl signal from a tungsten surface, Prince and Lambert (19) concluded that the interaction consists of dissociative adsorption followed by strong bulk diffusion. In contrast, no indication of a diffusion process is observed in the present study. Moreover, our activation energy for desorption of atomic chlorine is about a factor of two lower than the value suggested by Prince and Lambert (19).

Comparison of thermal desorption with molecular beam results.—Thermal desorption spectroscopy (TDS), a surface reaction analysis technique, provides kinetic informa-

tion on product desorption rates. In contrast, the molecular beam method provides data on the combined processes of adsorption, surface reaction, and desorption.

There are two distinct reaction paths for the formation of the reaction products in gas-surface interactions: Langmuir-Hinshelwood (LH), which is the result of surface reactions solely due to interaction between adsorbed species; and Eley-Rideal (ER), which involves collisions of an impinging gas with adsorbates to form a desorbed product. The latter is not detectable in TDS experiments. The proposed model, based on the molecular beam results for the production of WCl₄, utilizes only the ER reaction path. This model is consistent with the interpretation of TDS experiments (8) which suggest that the only desorption product observed on initially chlorine-saturated W(110) and W(111) is atomic chlorine. Had a LH step been involved, WCl₄ desorption should have been detected in the TDS experiments.

Comparison of the model with high pressure etching results.—In Ref. (1) the etching of tungsten films (about 100 nm thick, prepared by sputter deposition) was studied for samples positioned downstream from a Cl₂ plasma discharge at 200 mtorr and temperatures up to 420 K. In this configuration, ion-induced reactions are eliminated and the etching proceeds solely by thermal reaction between chlorine atoms and the film surface. It was concluded that the etch rate was proportional to the gas-phase Cl atom fraction and was temperature dependent with an activation energy of about 7.7 kcal/mol.

At these high pressures, the present model predicts that the surface is nearly completely chlorinated ($\theta \sim 1$). As a result, the reactivity becomes first order with respect to the beam intensity, which agrees with the high-pressure experimental data of Ref. (1).

The measurements of Ref. (1) show an increase in reaction probability from 3×10^{-5} to 1.5×10^{-3} as temperature is increased from 300 to 400 K. Application of the present model to the steady-state reaction of atomic chlorine and tungsten yields the following surface chlorine balance

$$I_1(1 - \theta) = 2k_r N^2 \theta^2 + k_d N \theta + 3\eta'_{er} I_1 \theta \quad [7]$$

where I_1 is the Cl(g) impingement rate from the gas

$$I_1 = \frac{P_{Cl}}{\sqrt{2\pi m_{Cl} kT}} \quad [8]$$

and P_{Cl} is the pressure of atomic chlorine in the reactor chamber downstream of the discharge [measured in Ref. (1) to be ~ 100 mtorr]. The impingement rate is determined to be $\sim 3.5 \times 10^{19}$ atom/cm²-s. Using this value and the reaction parameters from Table I in Eq. [7] permits the steady-state Cl-atom coverage to be calculated as a function of temperature; it decreases from 0.79 at 300 K to 0.76 at 400 K. With a constant nonmodulated beam (dc), the reaction probability for the model is equal to the ratio of the rate of production of WCl₄ ($\eta'_{er} I_1 \theta$) to the rate of impingement of atomic chlorine on the surface (I_1), or

$$\epsilon_{dc} = \eta'_{er} \theta \quad [9]$$

Using $\eta'_{er} = 3 \times 10^{-3}$ from Table I, the dc reaction probability is found to be nearly constant at 2.3×10^{-3} for temperatures between 300 and 400 K. The reaction probabilities

Table I. Parameters of the W/Cl₂ reaction model

Parameter	Pre-exponential factor	Activation energy (kcal/mol)
N	1.5×10^{15} atom/cm ²	—
η	1.0	0 ^a
η_{er}	4×10^{-4}	0 ^a
k_d	6×10^{12} s ⁻¹	59
k_r	2×10^{-2} cm ² /s	61(1-0.9 θ) ^b
η'_{er}	3×10^{-3}	0 ^a

^aAssumed.

^bThe zero-coverage value was determined as described in the text.

Table II. Desorption rate constants of atomic chlorine on tungsten

Tungsten surface	Binding energy (kcal/mol)	Pre-exponential factor (s ⁻¹)	References
(100), (111), (100)	94	10^{13} - 10^{14}	(7)
(110)	32	10^5	(8)
(110)	78	—	(9)
(100)	94	—	(9)
(100)	87	10^{13}	(10)
(100)	99	—	(11, 12)
(111)	92	10^{14}	(8)
(111)	94	—	(9)
Polycrystalline	59	6×10^{12}	This work

obtained in the experiments of Ref. (1) approach the value expected from the present model at high temperature (*i.e.*, 400 K), despite the fact that the model predictions involve extrapolation from low equivalent pressures ($<10^{-4}$ torr) to the pressures ($>10^{-1}$ torr) used in the etching apparatus (1). The decrease in reactivity with decreasing temperature observed in the higher pressure etching experiment may have been due to poisoning of the tungsten surface by background gas impurities since the base pressure was only $\sim 10^{-3}$ torr. Such poisoning is not present in the molecular beam experiments because of the high vacuum environment and the high temperature heat-treatment of the tungsten specimen employed just prior to reaction testing.

Comparison of the product distribution with equilibrium considerations.—The “quasi-equilibrium” model (20) may be applied to the reaction products and their temperature dependence for comparison with the molecular beam results. This model utilizes the principle of detailed balancing and the gas kinetic theory to predict the distribution of products in a gas-solid reaction. However, it cannot provide information on the reaction kinetics (*i.e.*, sticking probabilities) or the reaction mechanism. At Cl_2 pressures equivalent to the beam intensity used in the present tests, the model identifies WCl_4 as the chief product from 300 to ~ 800 K with Cl appearing above 1000 K. These predictions are in good agreement with the molecular beam results. Between 800 and 1000 K the quasi-equilibrium model predicts WCl_2 to be the main product. However this species was not observed in the present tests.

Summary

The reaction products of the low pressure W/Cl_2 and the W/Cl reaction are WCl_4 at low temperature and Cl at high temperature. A branched reaction model based on an Eley-Rideal mechanism satisfactorily describes the experimental data. The etch rate by chlorine atoms is a factor of approximately ten faster than that by molecular chlorine. The etch rates predicted by the model developed from the data are in agreement with the experimental results from a flowing afterglow study of tungsten etching in Cl/Cl_2 atmospheres.

Acknowledgments

This work was supported by the Director, Office of Energy Research, Office of Basic Energy Sciences, Materials Sciences Division of the U.S. Department of Energy under Contract no. DE-AC03-76SF00098 and the U.S. Department of Energy by the Lawrence Livermore National Laboratory under contract number W-7405-ENG-48.

Manuscript submitted Oct. 9, 1987; revised manuscript received March 17, 1988.

The Lawrence Berkeley Laboratory, assisted in meeting the publication costs of this article.

APPENDIX

Dissociation of the Incident Chlorine Flux

The intensity of the molecular beam impinging on the target with the discharge off, $[I_2]_{\text{off}}$, is calculated from the pressure in the source tube and gas kinetic theory. Since negligible source-tube pressure changes were observed when the RF was turned on, the mass balance on chlorine during the discharge on is given by

$$[I_2]_{\text{off}} = [I_2]_{\text{on}} + 0.5[I_1]_{\text{on}} \quad [\text{A-1}]$$

where $[I_2]_{\text{on}}$ and $[I_1]_{\text{on}}$ are the beam intensities of Cl_2 and Cl at the target with the discharge on.

The Cl^+ signal measured by the mass spectrometer, $[S_{\text{tot}}^{\text{Cl}^+}]$ is the sum of atomic chlorine ionization and dissociative ionization of molecular chlorine

$$[S_{\text{tot}}^{\text{Cl}^+}]_{\text{on}} = [S_{\text{Cl}}^{\text{Cl}^+}]_{\text{on}} + [S_{\text{Cl}_2}^{\text{Cl}^+}]_{\text{on}} \quad [\text{A-2}]$$

The signals on the right-hand side of Eq. [A-2] can be related to the beam intensities of molecular and atomic chlo-

rine striking the target and their common temperature, T , which may differ from room temperature because of heating in the discharge. The relations between signals and fluxes are

$$[S_{\text{Cl}}^{\text{Cl}^+}]_{\text{on}} = K \frac{\sigma_{\text{Cl}} b^{\text{Cl}^+} t^{\text{Cl}^+}}{V_{\text{Cl}}(T)} [I_1]_{\text{on}} \quad [\text{A-3}]$$

$$[S_{\text{Cl}_2}^{\text{Cl}^+}]_{\text{on}} = K \frac{a_{\text{Cl}_2}^{\text{Cl}^+} \sigma_{\text{Cl}_2} b^{\text{Cl}^+} t^{\text{Cl}^+}}{V_{\text{Cl}_2}(T)} [I_2]_{\text{on}} \quad [\text{A-4}]$$

where a , σ , b , t , and V are the cracking efficiency, ionization cross section, electron multiplier efficiency, quadrupole transmissivity, and the velocity of the gas, respectively. K is a species-independent instrumental factor.

Inserting Eq. [A-3] and [A-4] into Eq. [A-2] and dividing by the Cl signal when the discharge is off results in

$$\frac{[S_{\text{tot}}^{\text{Cl}^+}]_{\text{on}}}{[S_{\text{Cl}_2}^{\text{Cl}^+}]_{\text{off}}} = \sqrt{\frac{300}{T}} \left(\frac{[I_2]_{\text{on}}}{[I_2]_{\text{off}}} \right) + \left(\frac{1}{a_{\text{Cl}_2}^{\text{Cl}^+}} \right) \frac{\sigma_{\text{Cl}}}{\sigma_{\text{Cl}_2}} \sqrt{\frac{300 \cdot 35}{T \cdot 70}} \left(\frac{[I_1]_{\text{on}}}{[I_2]_{\text{off}}} \right) \quad [\text{A-5}]$$

where $a_{\text{Cl}_2}^{\text{Cl}^+} \sim 0.2$ for 70 eV electrons.

In addition, the ratio of the Cl_2^+ signal with the discharge on and off can be written as

$$\frac{[S_{\text{Cl}_2}^{\text{Cl}_2^+}]_{\text{on}}}{[S_{\text{Cl}_2}^{\text{Cl}_2^+}]_{\text{off}}} = \sqrt{\frac{300}{T}} \left\{ \frac{[I_2]_{\text{on}}}{[I_2]_{\text{off}}} \right\} \quad [\text{A-6}]$$

The left-hand sides of Eq. [A-5] and [A-6] consist of measured quantities. They vary with the gas pressure in the source tube and the discharge power. Equations [A-1], [A-5], and [A-6] can be solved for $[I_2]_{\text{on}}$, $[I_2]_{\text{off}}$, and T if the ratio of the atomic and molecular ionization cross sections is specified. With the discharge on and $(\sigma_{\text{Cl}}/\sigma_{\text{Cl}_2}) \sim 0.3$, the temperature of the beam at the target is found to be approximately room temperature. Dissociation of the beam is shown in Fig. 2 of the text.

REFERENCES

1. D. S. Fischl, G. W. Rodrigues, and D. W. Hess, *This Journal*, **135**, 2016 (1988).
2. R. H. Jones, D. R. Olander, W. J. Siekhaus, and J. A. Schwartz, *J. Vac. Sci. Technol.*, **9**, 1429 (1972).
3. J. A. Schwartz and R. J. Madix, *Surf. Sci.*, **46**, 317 (1974).
4. D. R. Olander, *J. Colloid Interface Sci.*, **58**, 169 (1977).
5. M. Balooch, W. J. Siekhaus, and D. R. Olander, *J. Phys. Chem.*, **88**, 3521 (1984).
6. A. Z. Ullman and D. R. Olander, *Int. J. Chem. Kinet.*, **8**, 625 (1976).
7. G. Bolback and J. C. Blais, *Surf. Sci.*, **137**, 327 (1984).
8. F. Bonczek, T. Engel, and E. Bauer, *ibid.*, **97**, 595 (1980).
9. M. C. Desjonqueres and D. Spanjaad, *J. Phys. C*, **16**, 3389 (1983).
10. H. M. Kramer and E. Bauer, *Surf. Sci.*, **107**, 1 (1981).
11. G. G. Price, K. J. Rawlings, and B. J. Hopkins, *ibid.*, **85**, 379 (1979).
12. K. J. Rawlings, G. G. Price, and B. J. Hopkin, *ibid.*, **100**, 289 (1980).
13. P. W. Tamm and L. D. Schmidt, *J. Chem. Phys.*, **51**, 5352 (1969).
14. D. R. Olander, T. R. Acharya, and A. Z. Ullman, *ibid.*, **67**, 3549 (1977).
15. M. P. D'Evelyn and R. J. Madix, *Surf. Sci. Rep.*, **3**, 413 (1984).
16. R. W. McCabe and L. D. Schmit, *Surf. Sci.*, **65**, 189 (1977).
17. C. T. Campbell and T. N. Taylor, *ibid.*, **122**, 119 (1982).
18. M. Balooch, W. J. Siekhaus, and D. R. Olander, *J. Phys. Chem.*, **90**, 1671 (1986).
19. R. H. Prince and R. M. Lambert, *Chem. Phys. Lett.*, **67**, 388 (1979).
20. J. C. Batty and R. E. Stickney, *J. Chem. Phys.*, **51**, 4475 (1969).